Characterizing Supersonic Jet Impingement Behavior

Aidan J. Fogleman*, John D. Weiss†, Wen Wu‡, and Dr. Surabhi Singh§
Embry-Riddle Aeronautical University, Daytona Beach, Florida, 32114, United States

Vertical/short takeoff and landing (V/STOL) aircraft such as the F-35B and AV-8B encounter significant stability and control challenges arising from exhaust-induced upwash and its interaction with the underside of the airframe. Although prior research has examined impinging jet behavior and ground effects in V/STOL operations, comparatively little work has investigated dual-flow exhaust configurations and their role in amplifying or mitigating upwash phenomena. This project therefore seeks to determine how interactions between a dual-flow exhaust system and a nearby surface influence upwash formation, shock structure evolution, and overall flow stability during V/STOL operations. To address this question, a modular supersonic impinging jet test stand was designed to emulate the F-35B's lift fan and main nozzle exhaust arrangement at laboratory scale. The test stand incorporates a Mach 1.67 converging-diverging (CD) nozzle (swappable with a Mach 1 converging-only nozzle) and an electric ducted fan (EDF), operating at a design gauge pressure of 70 psi and sized to maintain flow similarity based on publicly available aircraft engine data. Second-order computational fluid dynamics (CFD) simulations were performed to characterize impingement dynamics, shear layer evolution, and shock cell structure across varying standoff heights and configurations. These simulations were validated through schlieren imaging, with mesh-refinement studies planned to determine optimal grid density. Initial results from free-jet testing without the EDF have demonstrated strong agreement between simulated and experimental shock structures, supporting the validity of the simulations. Upcoming experiments will extend the analysis to impingement conditions, before integrating the EDF to replicate the full dual-flow configuration. Collectively, these results will clarify the influence of dual-flow exhaust systems on upwash behavior and highlight design considerations that could reduce associated stability problems in future V/STOL aircraft.

I. Nomenclature

A	=	nozzle cross-sectional area
A^*	=	sonic area
a	=	local sonic velocity
d	=	diameter
k_{factor}	=	geometric scaling factor
L_{char}	=	characteristic length
M	=	Mach number
p	=	static pressure
R	=	gas constant
Re	=	Reynolds number
T	=	static temperature
t	=	wall thickness
v	=	fluid velocity
γ	=	ratio of specific heats
ϵ	=	nozzle area ratio $\left(\frac{A_e}{A_t}\right)$
μ	=	dynamic viscosity
ρ	=	density

*Undergraduate Student, Aerospace Engineering Department, AIAA University Student Member 1864311.
†Undergraduate Student, Aerospace Engineering Department, AIAA University Student Member 1774343.
‡Graduate Student, Aerospace Engineering Department, AIAA University Student Member 1894264.
§Assistant Professor, Aerospace Engineering Department, AIAA Faculty Member 1374974.

Subscripts

a = ambient property
e = located at nozzle exit
t = located at nozzle throat
0 = total/stagnation property

II. Introduction

This paper details the design, construction, and preliminary testing of a supersonic impinging jet test stand by the Modal Analysis & Control of High-speed (MACH) Flow Lab at Embry-Riddle Aeronautical University (ERAU), as well as the potential for future research and applications. Said test stand was designed to interface with the MACH Flow Lab's blowdown supersonic wind tunnel to replicate the flow conditions created by the F-35B Lightning II's vertical/short takeoff and landing (V/STOL) thrust system, which features a thrust-vectored supersonic nozzle operating in tandem with a downward-facing lift fan, and allows the aircraft to hover in place or descend vertically. During V/STOL operations, these two jets interact with the ground and each other, resulting in complex upwash phenomena (such as strong pressure gradients and aeroacoustic feedback loops) that have the potential to cause adverse flight conditions and destabilize the aircraft [1, 2].

The problems faced by the F-35B are not new. Previous V/STOL aircraft such as the AV-8B Harrier II, Mirage IIIV, and Yak-141 have historically employed similar multi-flow configurations, but have also encountered difficulties as a result; the AV-8B, for example, experienced significant lift loss and stability issues during hover, due to flow entrainment arising from the impingement of its vertical jets upon the ground. These effects have only become more pronounced with the advent of more powerful fifth-generation aircraft such as the F-35B, making supersonic jet impingement a burgeoning topic of interest in the aerospace field [2]. The ultimate goal of this project is to visualize these flow interactions, so as to further characterize the behavior of supersonic dual-flow systems and investigate potential mitigation methods based on the results obtained therein.

III. Model Design

A. Flow Similarity

To ensure that the test stand would accurately mirror the F-35B's exhaust, a flow similarity analysis was conducted. Originally, said analysis was based on the exhaust properties at the aircraft's main engine nozzle exit; however, it was discovered that the actual values for these parameters are not publicly available, so a simplified cycle analysis of the Pratt & Whitney F135 engine (i.e., the F-35B main engine) was instead conducted based on published specifications for thrust and other performance metrics. The following table was obtained from [3]:

Table 1 Publicly available F-35B specifications.

V/STOL Propulsion System Design	
Maximum Thrust Class	182.4 kN
Intermediate Thrust Class	120.1 kN
Short Takeoff Thrust Class	181.2 kN
Hover Thrust	180.8 kN
Main Engine	83.1 kN
Lift Fan	83.1 kN
Roll Post	14.6 kN
Length	9.37 m
Main Engine Inlet Diameter	1.09 m
Main Engine Maximum Diameter	1.17 m
Lift Fan Inlet Diameter	1.30 m
Lift Fan Maximum Diameter	1.34 m
Conventional Bypass Ratio	0.56
Powered Lift Bypass Ratio	0.51
Conventional Overall Pressure Ratio	28
Powered Lift Overall Pressure Ratio	29

Using the values in Table 1, a MATLAB-based cycle analysis tool was developed based on standard turbofan engine models. Input values such as combustor exit temperature and nozzle pressure ratio were iterated until the calculated thrust relatively matched the main engine thrust (during hover) listed above; the other relevant engine values (such as p_e, T_e, and M_e, among others) were taken as outputs. The final values from this analysis are tabulated in Table 2.

Table 2 MATLAB cycle analysis results.

Cycle Analysis Script Output	
Thrust	83.6 kN
T_e	1212.5 K
p_e	36.8 kPa
M_e	1.6304

Once the F135's exit pressure, temperature, and Mach number had been estimated, it was decided whether dynamic similarity between the model and the actual engine could be achieved. Dynamic similarity is defined in [4] as matching Reynolds and Mach numbers between a sub-scale model and actual application; the former is defined as

$$Re = \frac{\rho v L_{char}}{\mu} \tag{1}$$

where, in this case, L_{char} is assumed to be the nozzle's exit diameter. Using Equation (1), the exit Reynolds number was calculated for the actual engine, and assumed to be equal to that of the model nozzle. In the latter case, L_{char} was assumed to be the nozzle's exit diameter of 1 in (0.0254 m) for simplicity; using this, the model's exit Re was calculated again using Equation (1) based on standard sea-level conditions, as well as expected flow properties from a compressed-air reservoir (i.e., the MACH Flow Lab's supersonic wind tunnel). This was then used as a basis to back-calculate the necessary exit velocity for the model nozzle to achieve the specified Re. The results of said calculations are shown in Table 3:

Table 3 Calculated values based on Re similarity.

Exit Condition	**F135 (During Hover)**	**Model Nozzle**
T_e [K]	1212.53	273.15
p_e [kPa]	36.780	0.4053
$R\left[\frac{J}{kg \cdot K}\right]$	231.92	287.06
μ [Pa·s]	4.653e-5	1.716e-5
$\rho\left[\frac{kg}{m^3}\right]$	0.1308	5.1690
$v_e\left[\frac{m}{s}\right]$	554.81	225.21
L_{char} [m]	1.105	0.0254
Re [--]	1.723e+6	1.723e+6

At this point, it was realized that to achieve Re similarity, the model nozzle's exit velocity would have to be approximately 225 m/s – well below the speed of sound at sea level (approximately 343 m/s), making it impossible to achieve full dynamic similarity with the chosen nozzle geometry (as M_e for the F135 was previously determined to be approximately 1.63). It was eventually decided that, while less ideal than full dynamic similarity, M_e similarity was more valuable for accurate evaluation of the impinging jet than Re similarity.

B. Nozzle/EDF Mount Design

The first actual component of the test stand to be designed was the mount for the nozzle & electric ducted fan (EDF). A custom mounting block was designed to allow either a converging-diverging (CD) nozzle or a converging-only nozzle, alongside the EDF, to interface with the rest of the test stand, serving as a structural adapter and simplifying alignment, installation, and repeatability when testing. The block was machined from a single piece of solid aluminum, with nominal outer dimensions of 3 in × 3 in × 2 in, and features a tapered internal passage that transitions from a 2-in NPT female thread at the inlet to a 1.5-in diameter outlet, which mates directly with a flange on the nozzle via 8 mounting threads. The mount also features recessed rectangular indentations to interface with the EDF manifold, as seen in Figs. 1 and 3.

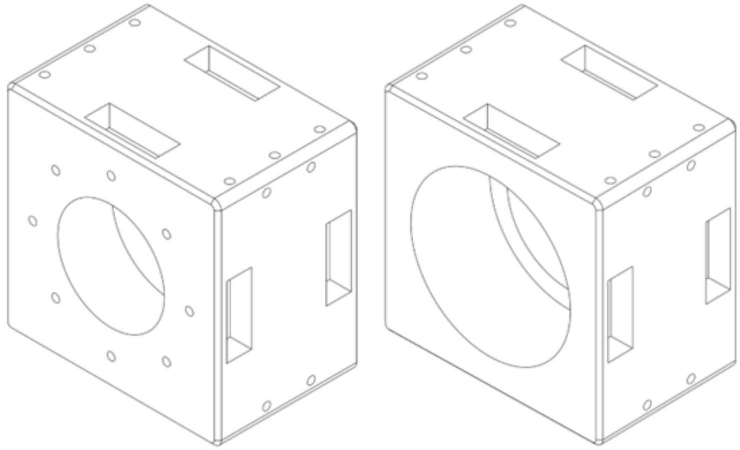

Fig. 1 The finalized nozzle manifold design.

Situated next to the nozzle mount is the EDF mount. While the nozzle was designed to emulate the vectored F135 thrust, the EDF was meant to mirror the F-35B's lift fan during V/STOL operations, allowing for replication of the dual-flow impingement phenomena observed in full-scale operation. A separate manifold was created to hold the EDF, and match the exit Mach number of the F-35B's lift fan. Since the propellor used to create the fan had a diameter of 4 in (0.1016 m), a separate nozzle had to be designed to reduce the exit area of the EDF. The geometric scaling factor was calculated using

$$k_{factor} = \frac{d_{nozzle,model}}{d_{nozzle,actual}} \tag{2}$$

and was found to be 0.023 m based on the model CD nozzle and F135 nozzle. The same scaling factor was used to calculate the required EDF exit diameter by rearranging Equation (2) into the form

$$d_{EDF} = d_{liftfan} k_{factor} \tag{3}$$

which yielded an EDF exit diameter of 0.0298 m. The distance between the centers of the nozzle and EDF exits was also scaled down using the same k_{factor}, and was determined to be 0.069 m using Equation (3). Additionally, an "X"-shaped motor housing and top ring were added to hold the motor and stabilize it during testing, as seen in Fig. 2.

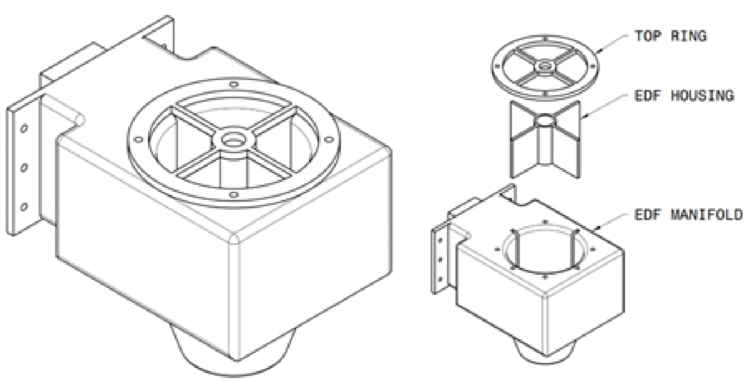

Fig. 2 The finalized EDF manifold design.

As mentioned previously, the two manifolds are connected to replicate the full dual-flow exhaust configuration, as seen in Fig. 3.

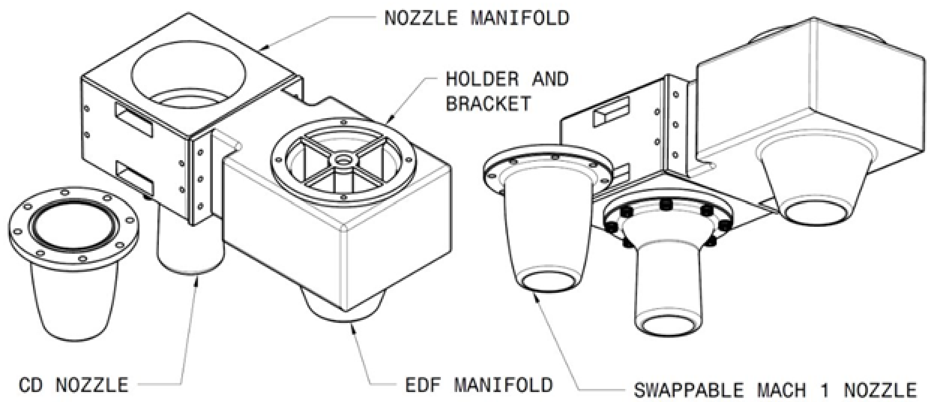

Fig. 3 The finalized design for the full nozzle/EDF mount, featuring both manifolds.

C. CD Nozzle Design

Once the mount had been designed, work could begin on designing the nozzles themselves. As mentioned previously, the CD nozzle's purpose is to smoothly accelerate compressed air to a calculated nominal Mach number of 1.6304, replicating the conditions produced by the F135's exit nozzle during V/STOL operations. The working fluid was assumed to be air, modeled as an ideal gas such that $\gamma = 1.4$ and $R = 287.05 \frac{J}{kg \cdot K}$; additionally, p_0 was chosen to be 70 psig (584.0 kPa(a)), d_e was chosen to be 1.000 in (0.0254 m), and t was chosen to be 0.100 in (2.54e-3 m).

Firstly, a preliminary analysis was conducted using quasi-one-dimensional flow assumptions and principles from isentropic compressible flow theory. ϵ was found using the area-Mach relation

$$\frac{A_e}{A^*} = \frac{1}{M_e}\left[\frac{2}{\gamma+1}\left(1+\frac{\gamma-1}{2}M_e^2\right)\right]^{\frac{\gamma+1}{2(\gamma-1)}} \tag{4}$$

where, assuming choked flow at the nozzle throat, A_t is equivalent to A^*, and thus $\frac{A_e}{A^*}$ is equal to ϵ. Using the target value of 1.6304 for M_e yields an ϵ value of 1.275, meaning $A_t = \frac{A_e}{1.275}$. Given an exit diameter of 1.000 in (i.e., an exit area of 0.785 in^2), then, results in a throat area of 0.616 in^2, corresponding to a throat diameter of approximately 0.884 in (0.0225 m).

While the quasi-one-dimensional model provided a useful initial approximation of the nozzle behavior, it operates under a number of simplifying assumptions that do not fully represent real-world supersonic flows; namely, the quasi-one-dimensional model does not account for multi-dimensional flow effects such as turning flow, oblique shock interactions, and boundary-layer growth, among others. To overcome these limitations, the method of characteristics (MOC), a common tool for designing supersonic nozzles, was utilized as described in [5] to generate a nozzle profile that would produce a smoother, shock-free flow field and more accurately achieve the desired exit conditions. The MOC approach yields significantly more optimized results than the simplified quasi-one-dimensional model, especially in supersonic flow regimes where multi-dimensional effects become prominent.

After conducting the MOC analysis, the overall CD nozzle design began to be finalized. A divergence half-angle of 5° was chosen, as this would in theory maintain near-isentropic expansion and nearly eliminate internal flow disturbances while also simplifying CNC manufacturing. The MOC contour was modeled in OnShape, and a smooth converging section was connected to it so as to cleanly accelerate the flow without forming any internal shocks. Care was taken to ensure a smoothly filleted throat region, as an overly sharp throat can often induce oblique shock formation in the nozzle diverging section. Additionally, a flange with 8 pre-tapped mounting holes was added to the face of the converging section to attach the nozzle to the test stand; a groove for an O-ring was also engraved into said flange to seal the flow inside the nozzle and prevent any leakage. The final CD nozzle design, as seen in Figs. 4 and 5, strikes an optimal balance between aerodynamic performance and ease of manufacturing. The nozzle was machined from 6061-T6 aluminum – selected for its strength-to-weight ratio, machinability, and capability to withstand extreme pressures without failing (such as those encountered by the nozzle during testing) – via CNC milling.

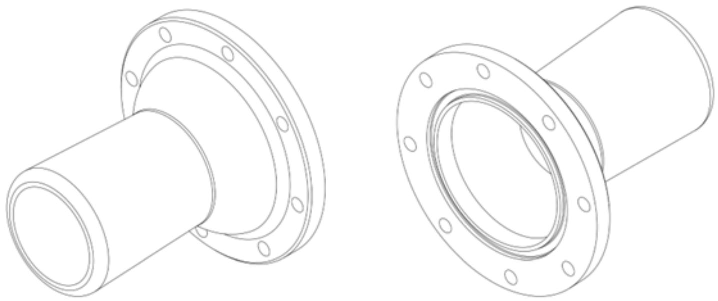

Fig. 4 The finalized design for the CD nozzle.

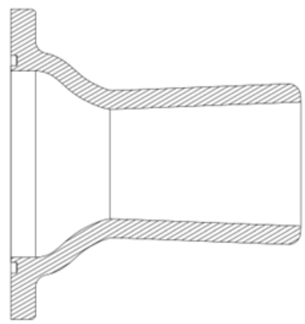

Fig. 5 A cross-sectional view of the CD nozzle contour.

D. Converging-Only Nozzle Design

In addition to the CD nozzle, a converging-only nozzle was designed to act as a reference geometry against which to contrast the results obtained from the former. Unlike the CD nozzle, the converging-only nozzle has no diverging section, and is thus only capable of accelerating the flow to sonic conditions at the throat/exit before it is released into the ambient environment. The same ambient and initial geometric conditions (i.e., γ, R, p_0, and t) were assumed for this nozzle as for the CD nozzle. To maintain consistency with the CD nozzle, d_e was kept at 1.000 in (0.0254 m); since, for a converging-only nozzle, the throat is the same as the exit (i.e., $d_e = d_t$), this nozzle's throat diameter exceeded that of the CD nozzle.

To achieve choked flow in the nozzle, and therefore Mach 1 at the throat, the ratio of p_0 to p_a (also known as the nozzle pressure ratio, or NPR) must satisfy the following inequality:

$$\frac{p_0}{p_a} \geq \left(\frac{\gamma + 1}{2}\right)^{\frac{\gamma}{\gamma - 1}} \tag{5}$$

When considering air as an ideal gas (i.e., $\gamma = 1.4$), this equation yields a minimum NPR of approximately 1.893; using a p_0 of 70 psig (84.7 psia) and assuming $p_a = 14.7$ psia yields an NPR of approximately 5.762, meaning that, assuming the proper upstream pressure is provided, the nozzle will be choked regardless of the throat/exit area. Generally speaking, the geometry of a nozzle's converging section is generally not of significant concern compared to the diverging section, so for a converging-only nozzle such as this one, less work was necessary to generate an optimal nozzle contour. A generic smooth contour was, as with the CD nozzle, generated in OnShape, containing an identical flange to allow mounting with the manifold; the nozzle was again CNC-milled from 6061-T6 aluminum, and can be seen in Figs. 6 and 7.

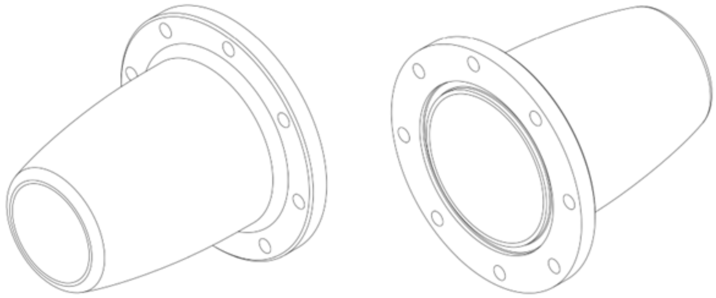

Fig. 6 The finalized design for the converging-only nozzle.

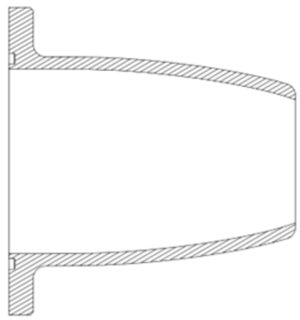

Fig. 7 A cross-sectional view of the converging-only nozzle contour.

E. Overall Test Stand Design

Upstream of the nozzle/EDF mount and the components themselves, the test stand also incorporates a solenoid valve and a ball valve in series as safety measures; the two valves provide a redundant shutoff method in case any hazards or other emergency issues arise during testing, and can be seen in Fig. 8.

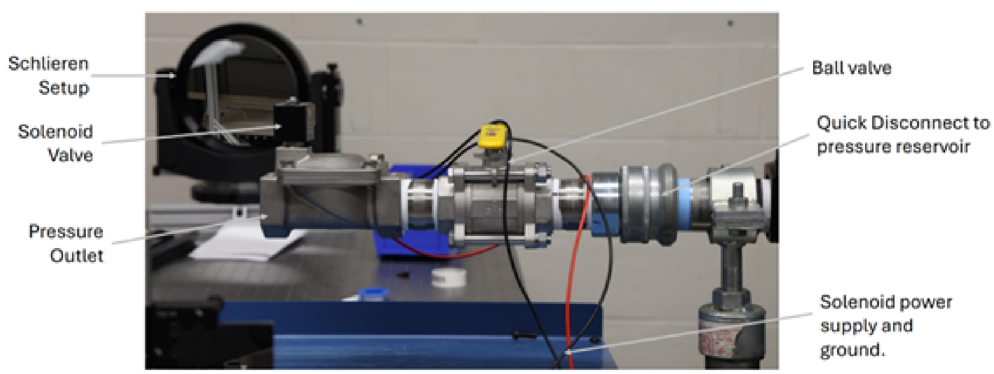

Fig. 8 A view of the valves upstream of the nozzle/EDF mount. Note that the right end is connected to the supersonic wind tunnel's pressure reservoir, and flow in this image therefore travels from right to left.

IV. Experimental Testing

A. Computational Fluid Dynamics

Due to manufacturing and shipping delays (namely, pertaining to the nozzles), physical experimentation was not possible for some time; for this reason, initial design validation consisted of computational fluid dynamics (CFD) simulations to model flow behavior before actual testing could be conducted. Said simulations were conducted using two-dimensional, steady-state models of the nozzle and EDF configurations, allowing for the modeling of shock structures and impingement behavior across a variety of test conditions; variables changed across simulations include impingement height, relative nozzle-fan positioning, and p_0. The Mach number and pressure distributions obtained from the CFD simulations not only helped inform experimental procedures, but also provided early insight into the flow's behavior.

The first step of the CFD analysis was to create a mesh to be analyzed. Two-dimensional profiles of the geometry of each nozzle were generated from their respective CAD models, and imported into Fidelity Pointwise. An unstructured triangular mesh was created with increased resolution near areas of interest such as the nozzle walls, throat, and exit to better capture viscous effects and shock formation, as seen in Figs. 9 and 10. Multiple meshes were created for each nozzle, modeling impingement distances of 2.5, 5.0, and 10.0 in; however, due to paper length constraints, it is not feasible to include images of all of them.

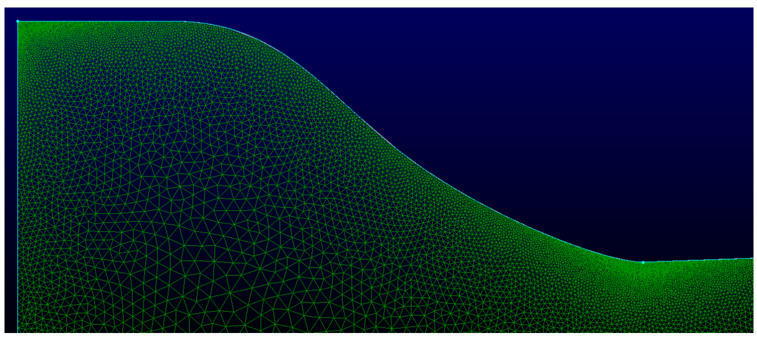

Fig. 9 A close-up screenshot of the mesh used to conduct CFD for the CD nozzle.

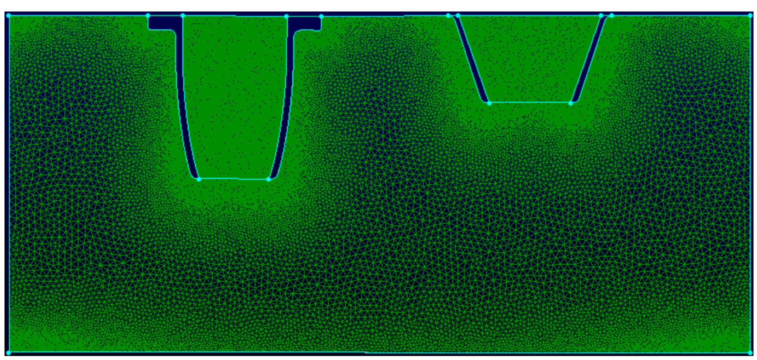

Fig. 10 A screenshot of the mesh used to study impingement with the converging-only nozzle, at an impingement distance of 2.5 in.

The generated meshes were imported into ANSYS Fluent for simulation, using a steady-state, density-based solver. The k-ω SST model was selected for turbulence modeling, as it excels at capturing boundary layer behavior in high-speed flows. The conservation of energy equation was enabled to account for thermal effects, and the working fluid was air (modeled as an ideal gas using the NASA 9-coefficient polynomial for thermodynamic properties); additionally, the Advection Upstream Splitting Method (AUSM) algorithm was enabled for capturing shock behavior and second-order upwind discretization for transport equations. The boundary conditions were defined as a total pressure inlet of 70 psig (482.6 kPa(g)) at the nozzle inlet, a uniform velocity inlet of 34.953 $\frac{m}{s}$ at the EDF inlet, a wall at the impingement surface, and pressure outlets at the other downstream boundaries. The turbulent intensity and viscosity ratios were set to 5% and 10%, respectively, across all inlets. Simulations were run using the implicit finite volume method, with a Courant number of 0.5 and maximum of 50,000 iterations, and contours of static pressure and Mach number were generated to characterize the flow's behavior as seen in Figs. 11 and 12. (Again, due to paper length constraints, it is unfortunately not feasible to show results for all trials or impingement distances.)

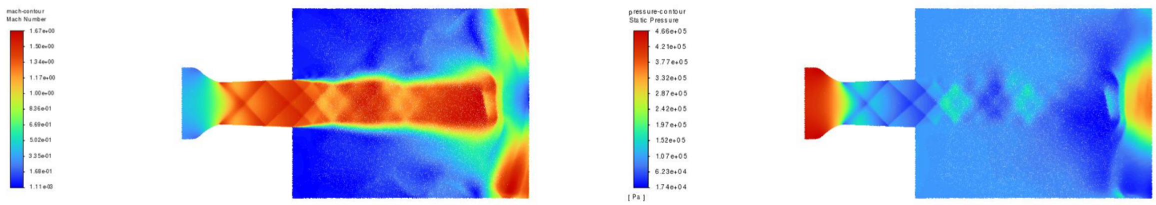

Fig. 11 Contours of Mach number (left) and static pressure (right) for the CD nozzle at an impingement distance of 5 in.

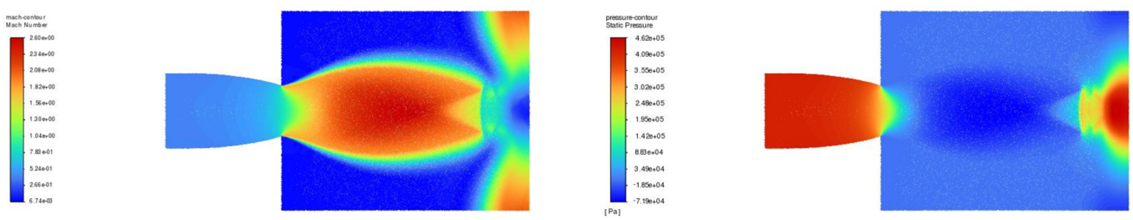

Fig. 12 Contours of Mach number (left) and static pressure (right) for the converging-only nozzle at an impingement distance of 5 in.

Despite the multiple steps taken to ensure smooth flow throughout the CD nozzle, there is still an oblique shock forming nearly immediately after the nozzle throat; this is thought to be the result of an overly violent turn between the converging and diverging sections, and potential improvements to the nozzle geometry remain an ongoing area of interest in this study.

B. Schlieren Imaging

Once the nozzles were received, physical testing could finally begin, but with a caveat: as of the time of writing, the EDF motor has still not been received, and efforts to design a physical impingement surface are ongoing. Because of this, all physical testing thus far has only dealt with free-jet testing of the nozzles only; despite not exactly matching the intended experimental setup, this still provides a valuable way to validate fundamental flow properties and establish a baseline against which the impingement experiments can be compared.

For the physical tests, the test stand was assembled as seen in Fig. 8, with the addition of the nozzle and its manifold on the downstream end. Tests were conducted for each nozzle at upstream pressures ranging from 10-70 psig; for the sake of brevity, this paper will focus only on the results obtained from the nominal upstream pressure of 70 psig. A pressure regulator upstream of the valves was set to 70 psig in accordance with the experiment procedures, and the supersonic wind tunnel's compressor was turned on until the pressure reservoir reached approximately 150 psig. A Z-type schlieren imaging system was focused on the nozzle exit, with a high-speed camera recording the flow. The solenoid valve was held open, and the flow was released using the ball valve for approximately 5 seconds (long enough for the flow to reach steady-state). The images were then offloaded from the camera onto a connected PC; selected images that were deemed to be particularly clear are shown in Figs. 13 and 14.

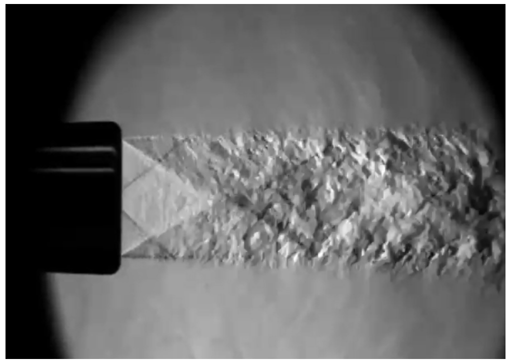

Fig. 13 Schlieren imaging of the CD nozzle at an upstream pressure of 70 psig.

Fig. 14 Schlieren imaging of the converging-only nozzle at an upstream pressure of 70 psig.

While schlieren images in and of themselves are not particularly useful for quantitative analysis, they serve to help validate the CFD results. The jet from the CD nozzle, for example, closely matches that found in Fig. 13, suggesting a fairly high degree of accuracy for other data gained from the simulation.

C. Next Steps

While much useful data has been gained from the work done so far, this study as a whole is far from complete. A suitable impingement surface is currently being designed, which will eventually allow for physical observation and measurement of impingement behaviors. Additionally, once the EDF is received, the test stand can finally be fully assembled, and real-life interactions of the dual flows can be observed, helping to achieve the overall goal of this study. Furthermore, depending on time constraints, the geometry of the CD nozzle may be altered in an effort to promote smoother flow acceleration and reduce or eliminate the oblique shocks seen in Figs. 11 and 13.

V. Conclusion

The work presented in this paper establishes a rigorously designed and partially validated experimental framework for investigating supersonic jet impingement in a dual-flow configuration representative of the F-35B's V/STOL propulsion system. Through compressible flow analysis, method-of-characteristics nozzle design, Reynolds and Mach similarity assessment, and second-order CFD modeling, a bench-scale test stand was developed to reproduce key exit conditions and shock structures associated with a Mach 1.63 exhaust. Schlieren imaging of free-jet nozzle flows demonstrated strong qualitative agreement with numerical predictions, thereby increasing confidence in the fidelity of the computational approach prior to full impingement and dual-flow testing. Although full dynamic similarity was not attainable, prioritizing Mach similarity preserves the major compressibility effects governing shock formation and impingement-induced pressure gradients. As the impingement surface and EDF integration are completed, the test stand will enable detailed investigation of shear-layer interaction, shock structures, and upwash amplification mechanisms in dual-flow systems. Ultimately, this work provides both an experimental platform and a scalable methodology for studying high-speed impinging jets, with direct implications for mitigating stability and control challenges in next-generation V/STOL aircraft.

Acknowledgments

The authors would like to thank Ryan Souza, Muhab Badawi, Samuel Gilbert, and Olivia Popdan for their work on the class project that would eventually become this study. Although they are no longer affiliated with the study in any official capacity, this study would not be possible without their efforts. Additionally, generative AI tools including ChatGPT were used occasionally to strengthen and/or refine certain sentences throughout the paper.

References

[1] Abdelkader, F., and Brown, M. R., "Flow structures and noise from a supersonic impinging jet," *International Journal of Numerical Methods for Heat & Fluid Flow*, Vol. 26, No. 8, 2016, pp. 2509–2527.

[2] Alvi, F. S., Ladd, J. A., and Bower, W. W., "Experimental and Computational Investigation of Supersonic Impinging Jets," *AIAA Journal*, Vol. 40, No. 4, 2002, pp. 599–609. https://doi.org/10.2514/2.1709.

[3] Pratt & Whitney, "F135 Specs Chart," United States Patent and Trademark Office, 2012. URL https://ptacts.uspto.gov/ptacts/public-informations/petitions/1476834/download-documents?artifactId=SfieZYkZxBtaDWFoZf8bQSk2W6j-ZDqV5nB2Kgwx3YyUiUZZL_VF-lI, accessed 14 Feb 2026.

[4] Leishman, J. G., *Introduction to Aerospace Flight Vehicles*, 4^{th} ed., EaglePubs, 2026. https://doi.org/10.15394/eaglepub.2022.1066.

[5] Anderson, J. D., *Modern Compressible Flow: With Historical Perspective*, 4^{th} ed., McGraw-Hill Education, 2021.